Engineered Underwater Vehicle for Ocean Litter Mapping

Daniel Kim[*]

Los Alamos High School, Los Alamos, NM, USA

ABSTRACT

This project explores the possibilities of pairing an autonomous underwater vehicle (AUV) with a deep-learning computer vision model for marine debris mapping. A cost-effective, 3D-printed AUV with a motorized ballast system was designed to collect underwater footage continuously at various depths for several weeks. A simulated underwater environment using hardware-in-the-loop (HIL) procedures was used to test and evaluate the AUV. A trash detection machine learning model was developed to analyze the footage for underwater litter. To assess the accuracy and capabilities of the trash detection model, footage from various underwater vehicles was compiled and run through the model, yielding five areas of highly concentrated ocean debris at depths of 500–800 m below the surface. This study highlights how many pieces of marine debris—undetectable by satellite data—can be mapped and categorized with the proposed AUV and trash detection model.

KEYWORDS: Autonomous underwater vehicle, Hardware-in-the-loop, Tracking and mapping, Marine debris, Real-time object detector, Machine learning.

1 INTRODUCTION

The use of plastics in the past 65 years has significantly outpaced the use of all other materials. Of the 8.3 billion metric tons of plastic ever produced, only 2500 metric tons are currently in use (Geyer et al., 2017). These plastics are the most dominant type of litter found in our oceans and contribute to the 244,000 metric tons of marine debris (Parker, 2022).

The issue has already caused substantial ecological and economic problems. Microplastics, shown to alter animal reproductive and metabolic endpoints, have been found in species intended for human consumption or those playing critical ecological roles (Galloway et al., 2017). Furthermore, microplastic accumulation in the oceans has been shown to cause $500–$2500 billion in loss of ecosystem services (Beaumont et al., 2019).

Although significant attention has been given to floating ocean litter (Eriksen et al., 2014), the distribution of macro-litter across the world is still relatively unknown (Galgani, 2015). However, benthic regions of coastlines have been shown to reach concentrations of up to 1.3 million items/km^2 (Pierdomenico et al., 2019), and plastics have been found to occur commonly in the benthos (Backhurst and Cole, 2000; Katsanevakis et al., 2007; Stefatos et al., 1999). Moreover, de-fouling of benthic litter from foulants and other organisms can decrease the density of the items, causing the debris to return to the surface and creating litter distributions across all depths of the ocean (Andrady, 2011). Therefore, methods to measure litter concentrations at all depths of the ocean are required.

Furthermore, current mapping methods are either inefficient or not comprehensive. One of the largest garbage patches in the world, the Great Pacific Garbage Patch, was mapped using a fleet of 18 vessels and 642 surface nets (Lebreton et al., 2018). This method created a comprehensive understanding of the largest garbage patch in the world but required vast resources and labor for a single assessment. The ceaseless movement of ocean debris requires continuous observation, but the use of large resources for one measurement is not sustainable. The Satellite Triangulated Sea Depth (SaTSeaD) model has offered a more cost-effective approach through satellite imagery but is limited to a depth of 30 m in clear waters (Palaseanu-Lovejoy et al., 2023).

The purpose of this study is to evaluate the use of an autonomous underwater vehicle (AUV) and a trash detection machine learning (ML) model to assist in marine litter quantification. AUVs are commonly employed for environmental inspections, such as tracking fish populations (Powell, 2022) and monitoring ocean temperatures, and have been shown to outperform surface vessels in underwater tracking and telemetry (Eiler et al., 2014). Moreover, AUVs are capable of surveying and capturing footage of different marine environments at depths up to 6000 m (Seafloor Mapping AUV, n.d) for ranges of over 2000 km (Long Range AUV (LRAUV), n.d.). Unlike satellites, AUVs allow for metrics to be collected at various depths, and contrary to current surface net and trawl quantification methods, AUVs are cost-effective and require very little manpower. Using an ML model, the footage collected by the AUV can be analyzed for ocean litter within most depths of the ocean, which can be used to build a comprehensive map of marine debris.

Using this method, the performance and capabilities of an engineered AUV are evaluated and open-sourced underwater video datasets are analyzed to create a model of ocean litter off the coast of Kamaishi, Japan. Using the ML model, a novel method of using AUVs to collect data on the scope of marine debris was assessed.

2 METHODOLOGY

2.1 Design of AUV

The AUV is based on the concept of an underwater glider, which is a robotic vehicle originally designed by Douglas Webb for cost-effective data collection in remote locations (Schofield et al., 2007). Underwater gliders do not have propellers or engines; they utilize changes in buoyancy to move up and down which creates lift to propel the vehicle forward. This method allows for the glider to operate for days, weeks, or even months autonomously before being recovered for data.

The AUV was first designed in computer-aided design (CAD) and 3D-printed. Each component of the AUV was a separate, modular design, which was then assembled onto a steel rod backbone. The entire assembly was then slid into a 102 mm × 914 mm clear PVC tube and was sealed with an O-ring endcap. Each of the 3D-printed modules was manufactured in polylactic acid (PLA), with high infill to increase the density of the vehicle. Because the inner printed parts are independent of the outer PVC tube, none of the inner components required waterproofing. The design's use of 3D-printed components allowed for easy modularity and cost-effective, repeatable manufacturing, resulting in a low overall cost.

The AUV was assembled using the 3D-printed parts and had a width of 10.16 cm, a wingspan of 0.72 m, and a length of 1.08 m. Initially, the weight of the vehicle was insufficient to sink, thus 3.63 kg of copper-plated lead weights were added to the interior of the AUV to make it neutrally

buoyant, giving it a final mass of 6.63 kg.

The AUV control board, the circuit board that operates the vehicle, was first designed and developed in electronic computer-aided design (ECAD) and then outsourced for fabrication by JLCPCB. Once the bare printed circuit board (PCB) was fabricated, individual integrated circuits were soldered using reflow. The microcontroller used on the control board was the Teensy® 4.1 (Teensy® 4.1, n.d), featuring the Arm® Cortex-M7 processor (Cortex-M7, n.d) at 528 MHz and 1024 kB of memory. The software that operated the control board was developed in C++ and a complementary graphical user interface (GUI) was developed in Typescript.

2.2 Trash Detection Model

The trash detection model was built on YOLOv5, an open-source ML framework. The dataset used to train the neural network was the Trash ICRA-19 dataset (Fulton, 2019), which contained 5700 annotated images of underwater trash. The training was performed on a Google Colab server with an NVIDIA Tesla T4 with 16 GB of memory and 2560 Compute Unified Device Architecture (CUDA) cores. Google Colab is a free cloud computing service offered by Google. Four different neural networks were trained and evaluated to find the best-suited model for trash detection. Table 1 summarizes the four different models. Once the models were trained, validation and deployment of the models were performed on a local server featuring the NVIDIA 1650Ti with 4 GB of memory and 896 CUDA cores.

Model	Parameters (millions)	Floating-point operations per second @ 640 pixels (billions)
YOLOv5n	1.9	4.5
YOLOv5s	7.2	16.5
YOLOv5m	46.5	49.0
YOLOv5l	86.7	109.1

Table 1: The four models trained for trash detection. The model that showed the highest accuracy is used for trash detection.

3 RESULTS AND DISCUSSION

3.1 Component Design for AUV

The AUV consists of four key components: a ballast tank to control buoyancy, a microcontroller system to control and operate the vehicle, aluminum wings placed at the center of mass to push the vehicle forward when rising and sinking, and a camera module to collect video footage of the surroundings (Figure 1).

3.1.1 Ballast System

The buoyant force, F_B, exerted on the vehicle is equivalent to the weight of the volume of water displaced by the vehicle. If the buoyant force is greater than the weight of the vehicle, F_W, the vehicle floats. Without lift, the weight of the vehicle is greater than the buoyant force, and the vehicle sinks. The AUV controls its weight by using a ballast tank. By pulling in water from its surroundings, the AUV increases in weight and can sink, and by pushing that water out and replacing the volume with decompressed air, the AUV floats.

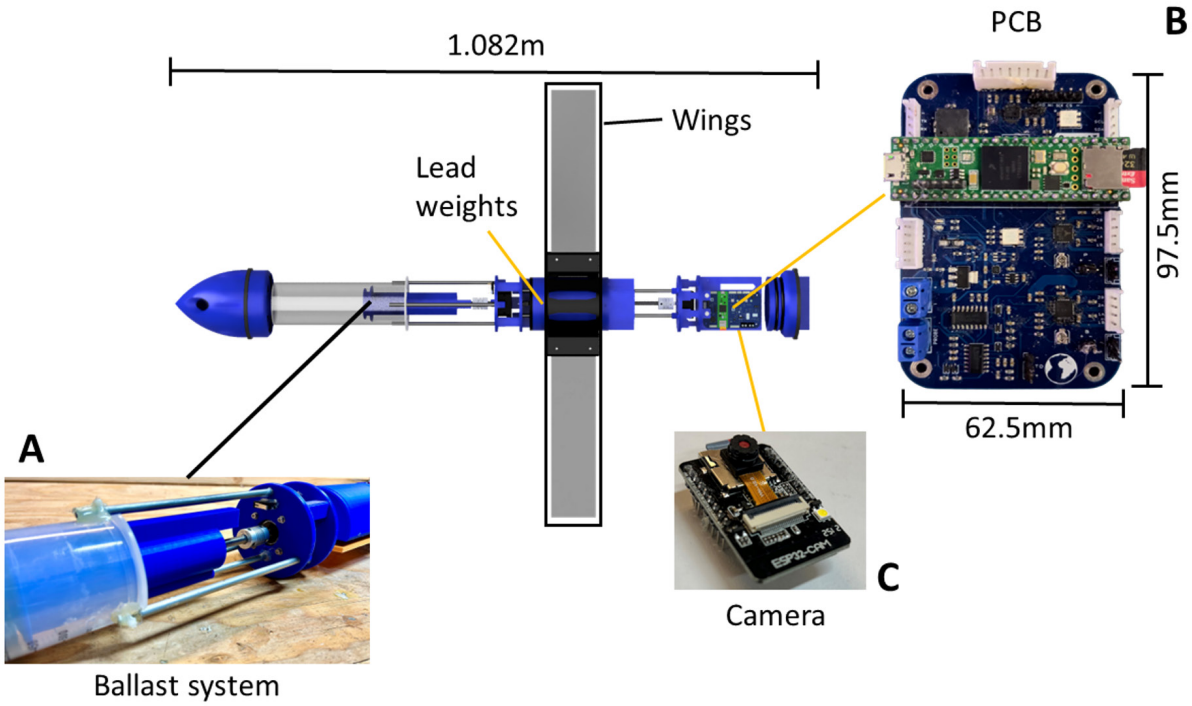

Figure 1: The AUV with its key components. (A) Ballast system used to control the buoyancy of the vehicle; (B) PCB for vehicle operation and sensor data collection; and (C) Camera board that captures footage of the underwater surroundings.

For the AUV in this study, the ballast system utilizes a 550 mL syringe with a plunger driven by a stepper motor running at 1 A to provide up to 16 N·cm of torque (Figure 2C). A threaded rod is connected to the stepper motor (Figure 2A) which pushes the syringe plunger in and out. The high accuracy of the stepper motor allows for fine-tuning adjustments to the amount of water in the tank to be controlled with very low power consumption. However, unlike servo motors, stepper motors provide no positional feedback, thus a limit switch is added to the end of the plunger's range of motion. By pulling the plunger until the limit switch is pushed (Figure 2B), the position of the plunger can be determined. The ballast assembly was able to pull in 450 mL of the 550 mL capacity, allowing for an additional 0.450 kg of water to be added to the AUV.

To test the ballast system, the AUV was placed in a local lake and was programmed to continuously fill and empty the ballast tank to sink and float. Initially, the AUV was too buoyant to sink, so an additional 308 g of lead was added to the rear of the AUV for a final mass of 6.629 kg. Lead was chosen due to its high density and relatively low cost. The lead was copper-plated to reduce the environmental and safety hazards associated with it. After the addition of the extra weight, the AUV was able to control its buoyancy with the ballast system and repeatedly float and sink (Figure 3). During the field test, the AUV was able to repeatedly reach the bottom of the lake at a depth of 2 m and resurface, while collecting sensor data.

During the field test, data from the accelerometer, gyroscope, and magnetometer were collected (Figure 4). Large amounts of linear acceleration were observed due to water currents applying forces to the vehicle. Angular speed was most significant in the Y direction, as the vehicle's front tilted down while sinking and up while floating. Since the vehicle's orientation relative to Earth did not significantly change much throughout the test, magnetic field readings stayed relatively level.

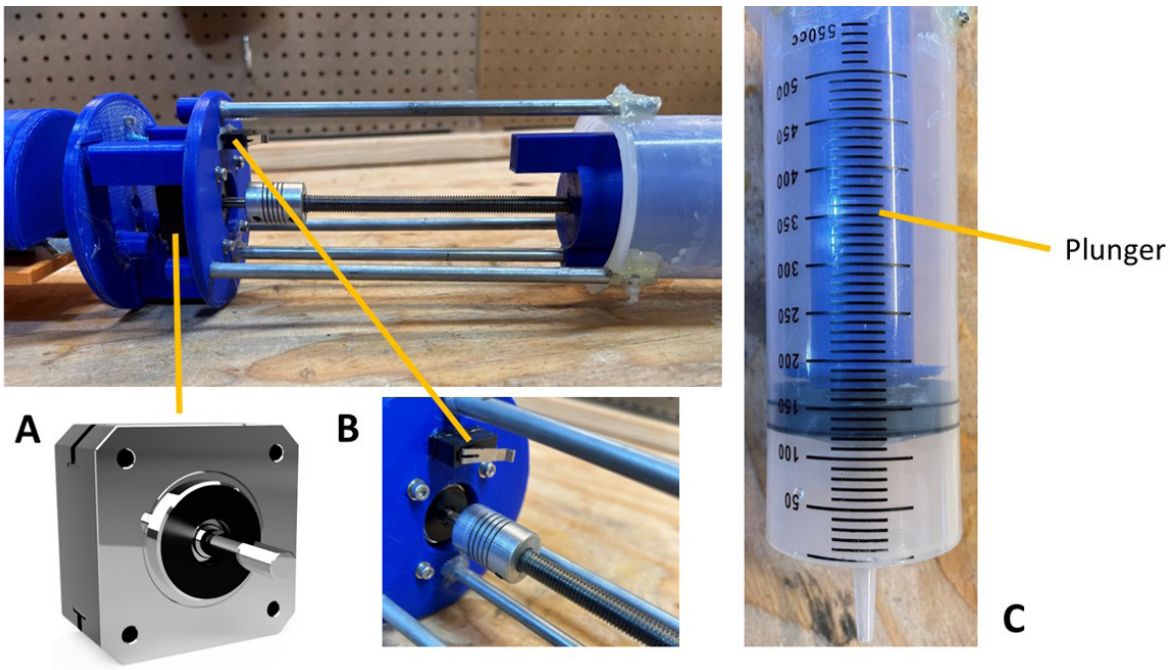

Figure 2: The AUV's ballast system. (A) Stepper Motor; (B) Limit Switch; and (C) Ballast Tank.

Figure 3: Field test of the AUV's ballast system.

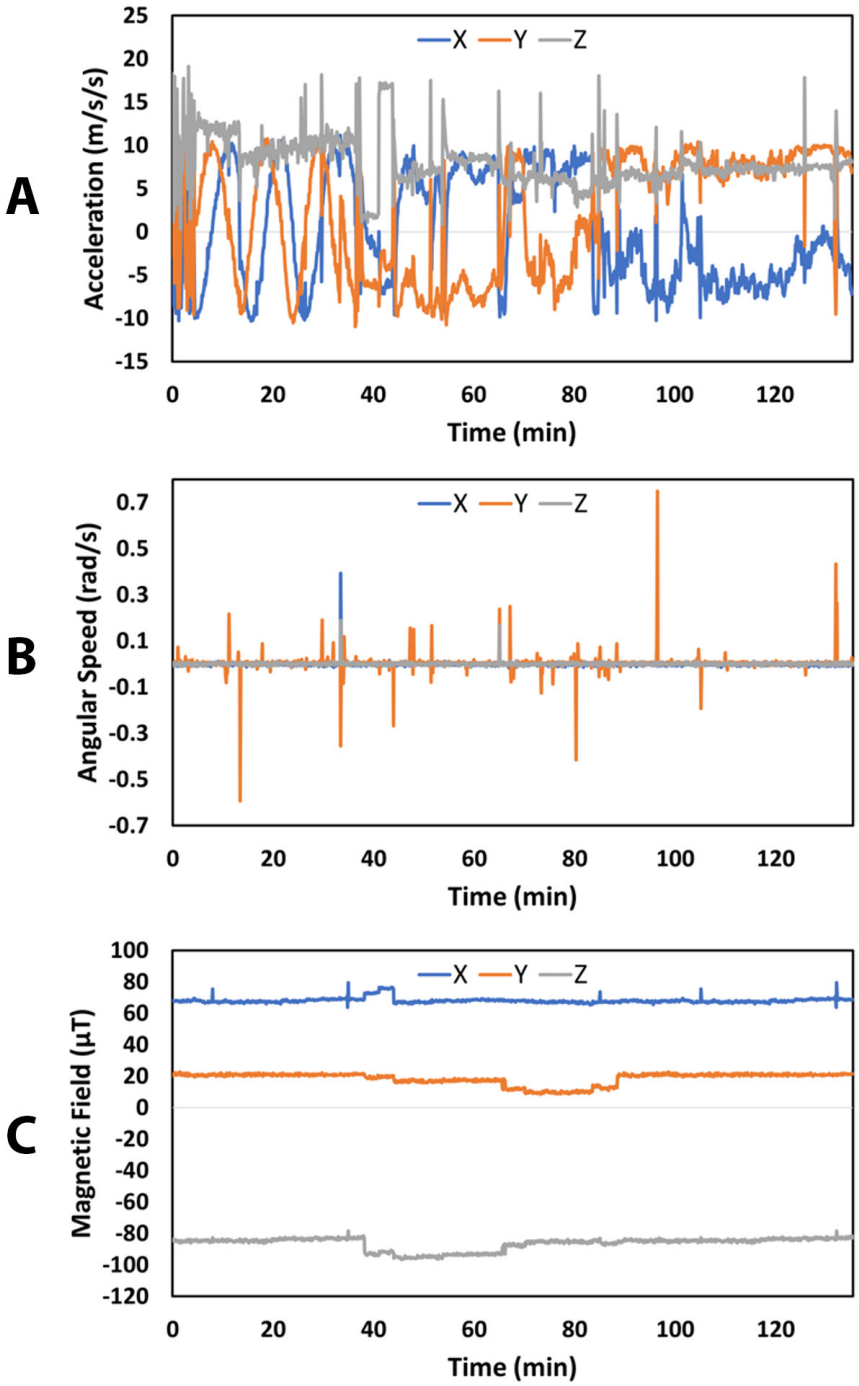

Figure 4: Accelerometer (A), gyroscope (B), and magnetometer (C) data were collected during the field test.

Depth was also estimated using the external pressure transducer (Figure 5). Throughout the test, the vehicle was programmed to repeatedly sink and float for 135 minutes. 70 minutes into the test, the speed of the ballast system's stepper motor was increased, which increased the sinking and resurfacing rate.

Data from the accelerometer, gyroscope, magnetometer, and pressure transducer were all measured at an average of 5400 Hz throughout the field test.

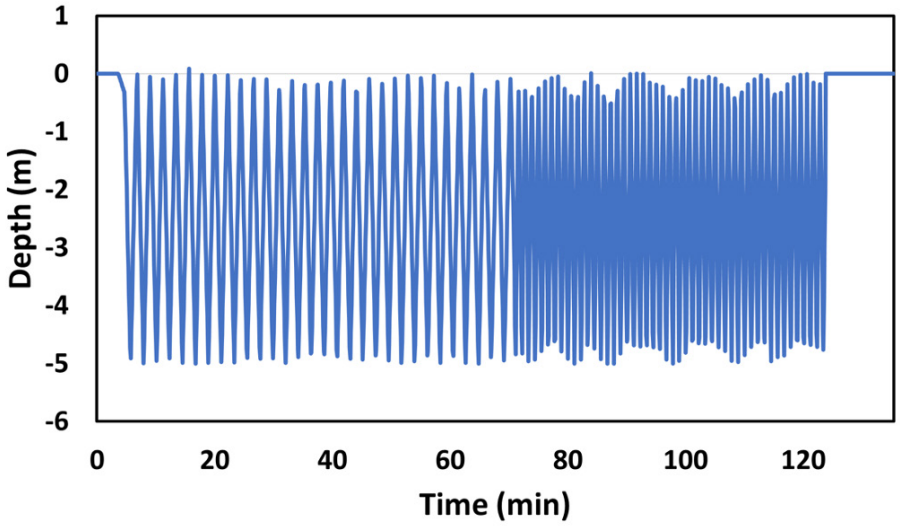

Figure 5: Calculated depth measurements throughout the test. After 70 minutes, the speed of the ballast system's stepper motor was increased to increase the rate of sinking and resurfacing.

3.1.2 AUV Control System

To read sensor data, control and navigate the AUV, and perform telemetry, a custom-printed circuit board was designed and assembled (Figure 6). At its core, the control system has a 528 MHz microcontroller unit that runs the AUV control software and controls all aspects of the vehicle.

To measure the orientation, relative speed, and position of the vehicle, the control board features an accelerometer, gyroscope, and magnetometer.

The board also includes a total dissolved solids (TDS) sensor to measure external solute concentrations. The TDS sensor calculates the concentration of solutes within the AUV's environment by measuring the current across two electrodes providing 3 V power at 50 Hz. The excitation source is alternating instead of direct current to prevent the sensor from polarization by preventing the buildup of charged particles on the electrodes. Because the conductivity of water increases as temperature increases, a thermistor is installed next to the TDS probe to calculate a more accurate reading.

To collect data needed for marine litter mapping, a GPS and external pressure sensor are connected to the board. These two sensors allow for the location and depth of any detected litter to be identified. All data collected from these sensors are logged onto a microSD card. The ballast tank is controlled through a stepper motor, which the control system operates using a stepper motor driver.

Because most radio frequencies greater than 1 MHz do not work at distances greater than 10 m underwater (Qureshi, 2016), the control board allows for wired connections through the serial peripheral interface (SPI) or inter-integrated circuit (I2C) protocols. Although not implemented, connections to external modules on the surface (using tethered buoys) would allow for telemetry and GPS data to be transmitted and received. The SPI and I2C interfaces also allow for other additional components to be added to the AUV framework, such as auxiliary sensors or cameras.

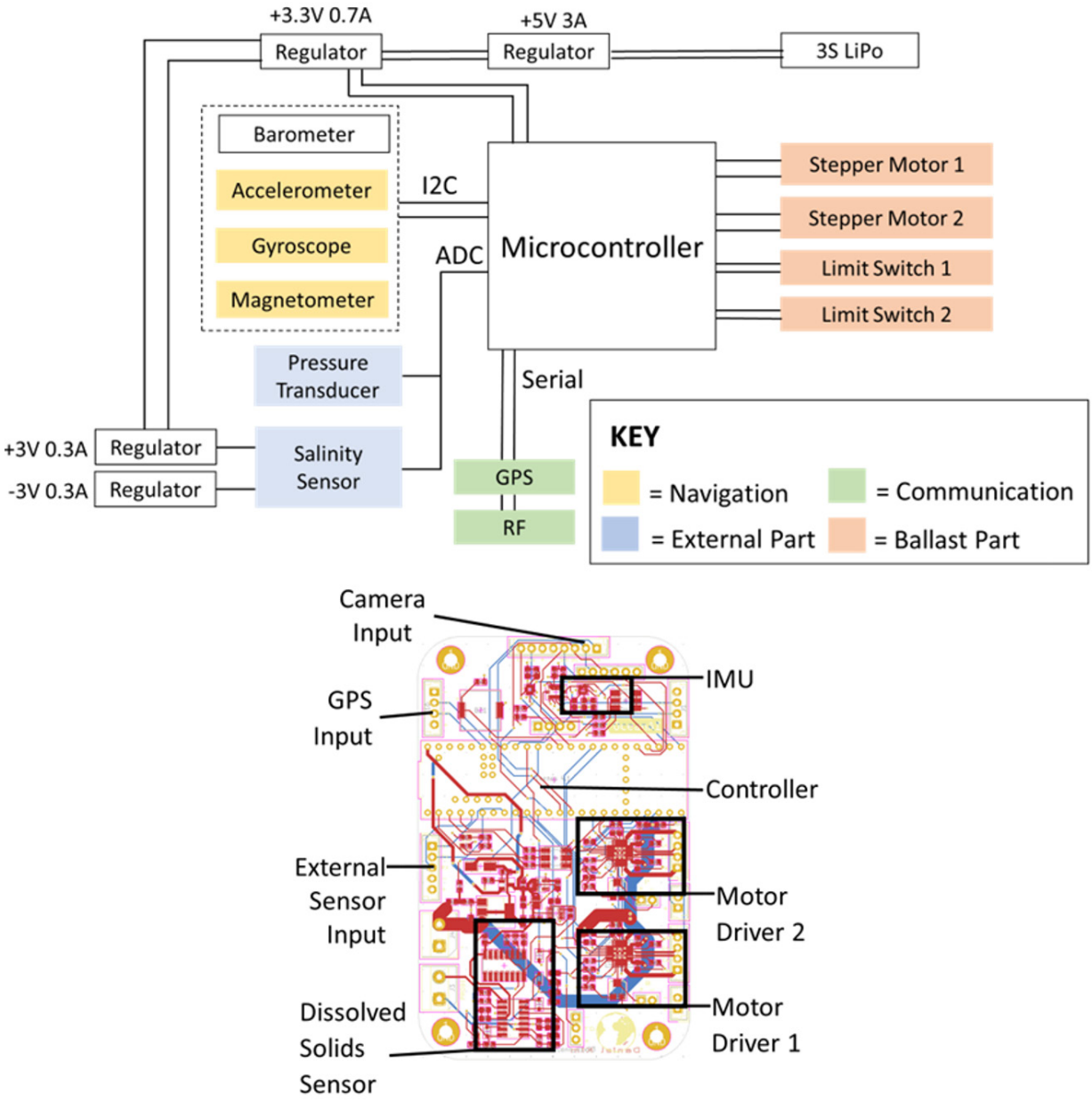

Figure 6: The components of the control board (top) and the labeled ECAD model of the control board (bottom).

3.1.3 Camera System

Although the main control board allows for an external camera module to be connected, image processing and logging are very CPU- and memory-intensive operations. Thus, a separate module was added to collect footage of the AUV's surroundings. The ESP32-S microcontroller with the OV2640 2-megapixel camera was chosen to collect footage of the AUV's surroundings (Figure 1C). The 32-bit ESP32 microcontroller runs at 240 MHz and features 2 cores and 520 kB of RAM, which is sufficient to capture video footage continuously and save it to a microSD card. The small size of the module (27 mm × 49 mm × 5 mm) allows for multiple camera units to be set up within the AUV, which can provide multiple camera angles.

3.1.4 AUV Control Software

Although the control system and camera system provided the hardware to operate the AUV, respective software had to be developed to run the control system. The software controls everything from the stepper motors to drive the ballast tank to the data collection and logging. The AUV control software is written in C++ and has two key aspects: sensor data collection and data logging/telemetry.

3.1.4.1 Sensor Data Collection

The AUV had seven key sensors that collected data about the state of the vehicle. The TDS sensor measures the number of solutes in the environment in conjunction with an external temperature and pressure sensor, while an accelerometer, gyroscope, magnetometer, and GPS were used to measure orientation and provide an estimate of the AUV's position.

External pressure readings provide accurate measurements of the depth of the vehicle. The pressure transducer outputs a simple analog output directly proportional to the pressure of the environment. The accelerometer, gyroscope, and magnetometer, (collectively referred to as the inertial measurement unit or IMU here) are each separate devices that provide readings to the microcontroller through the I2C communication protocol. For positioning, the AUV utilizes GPS data for absolute positioning and the IMU for localization. The GPS module provides horizontal positioning up to 2.5 m in accuracy at 10 Hz while the IMU provides accurate horizontal positioning through dead reckoning. Using GPS, pressure measurements, and the IMU, the position of the AUV in all three dimensions can be estimated. Although the Kalman Filter (Kalman, 1960) has become the accepted algorithm for most orientation estimates (Barshan and Durrant-Whyte, 1995; Foxlin, 1996; Luinge et al., 2003; Marins et al., 2001), the Madgwick algorithm was used for orientation estimation due to its lower static and dynamic root-mean-square errors (Madgwick et al., 2011).

3.1.4.2 Data Logging and Telemetry

During deployment, data is serialized onto a microSD card in the JSON format. A converter was also developed in C++ to convert the JSON data into more easily readable formats, such as CSV. Data is transmitted to an external GUI through the universal asynchronous receiver-transmitter (UART) protocol. The GUI is built in Typescript and provides live data feeds from the sensors allowing for control over the AUV's ballast system. Telemetry could be sent wirelessly through a tethered buoy but is sent directly through a wire directly connected to the control board during AUV testing.

3.2 Hardware-In-The-Loop

After designing and assembling the AUV and its respective software, extensive testing was required to evaluate its effectiveness. Unfortunately, many garbage patches exist in the middle of the ocean and the means of testing this application are not usually available. To overcome this challenge, a method called hardware-in-the-loop (HIL) was adopted to test the AUV. HIL testing simulates reality by feeding real signals through the platform while test and design iteration takes place. HIL allows for comprehensive testing of complex systems through many possible scenarios without spending time and money associated with real-world tests (What Is Hardware-In-The-Loop?, n.d.) The GUI read back sensor data and HIL data, allowing for adjustment of the stepper

motors to tune the vehicle. These tests evaluated the functionality of the sensors and mechanical aspects of the AUV, while also assessing the abilities of the software and control board to operate the AUV.

3.3 Trash Detection Model

The trash detection model locates and classifies litter in an image or video using a deep neural network. For each image or frame of a video, the model outputs a predicted bounding box surrounding the piece of litter. Once the AUV is recovered, the footage and sensor data are run through the model. If a piece of litter is detected, the model extracts the respective depth and GPS data, which can be used to build a comprehensive map of ocean litter. The trash detection model developed in this research has one class, enabling it to identify the presence or absence of trash in each image. The training was done on the Trash ICRA-19 Dataset (Fulton, 2019) which contained 5700 images of underwater trash, each of which was annotated with a ground truth bounding box that enclosed the litter within the image.

3.3.1 Training

Before the model could be deployed, it needed to be trained on a large dataset. For training, four different convolutional neural networks (CNNs) were used: YOLOv5n, YOLOv5s, YOLOv5m, and YOLOv5l (Jocher, 2023). Three metrics were used to determine which model to use. The mean average precision (mAP) was measured to determine the precision and recall of the model (Beitzel et al., 2009), the training loss was measured to see how well the model fit the training data, and the validation loss was measured to see how well the model generalized to new, unseen data.

Table 2 and Figure 7 show the different metrics of each of the four CNNs that were trained throughout the 200 epochs for which the model was trained. The YOLOv5l model exhibited the highest mAP and the lowest training and validation loss and was chosen as the best model to use.

	YOLOv5s	**YOLOv5n**	**YOLOv5m**	**YOLOv5l**
mAP (best)	0.706	0.720	0.759	0.774
mAP (average)	0.548	0.554	0.612	0.616
Training loss (best)	0.105	0.105	0.105	0.105
Training loss (average)	0.059	0.059	0.056	0.056
Validation loss (best)	0.105	0.105	0.105	0.105
Validation loss (average)	0.059	0.059	0.056	0.056
Percent Difference (best training vs. best validation)	0.000	0.000	0.002	0.000

Table 2: Best and average mAP, training loss, and validation loss for each neural network model. The percent difference defines the difference between the best training and validation loss metrics.

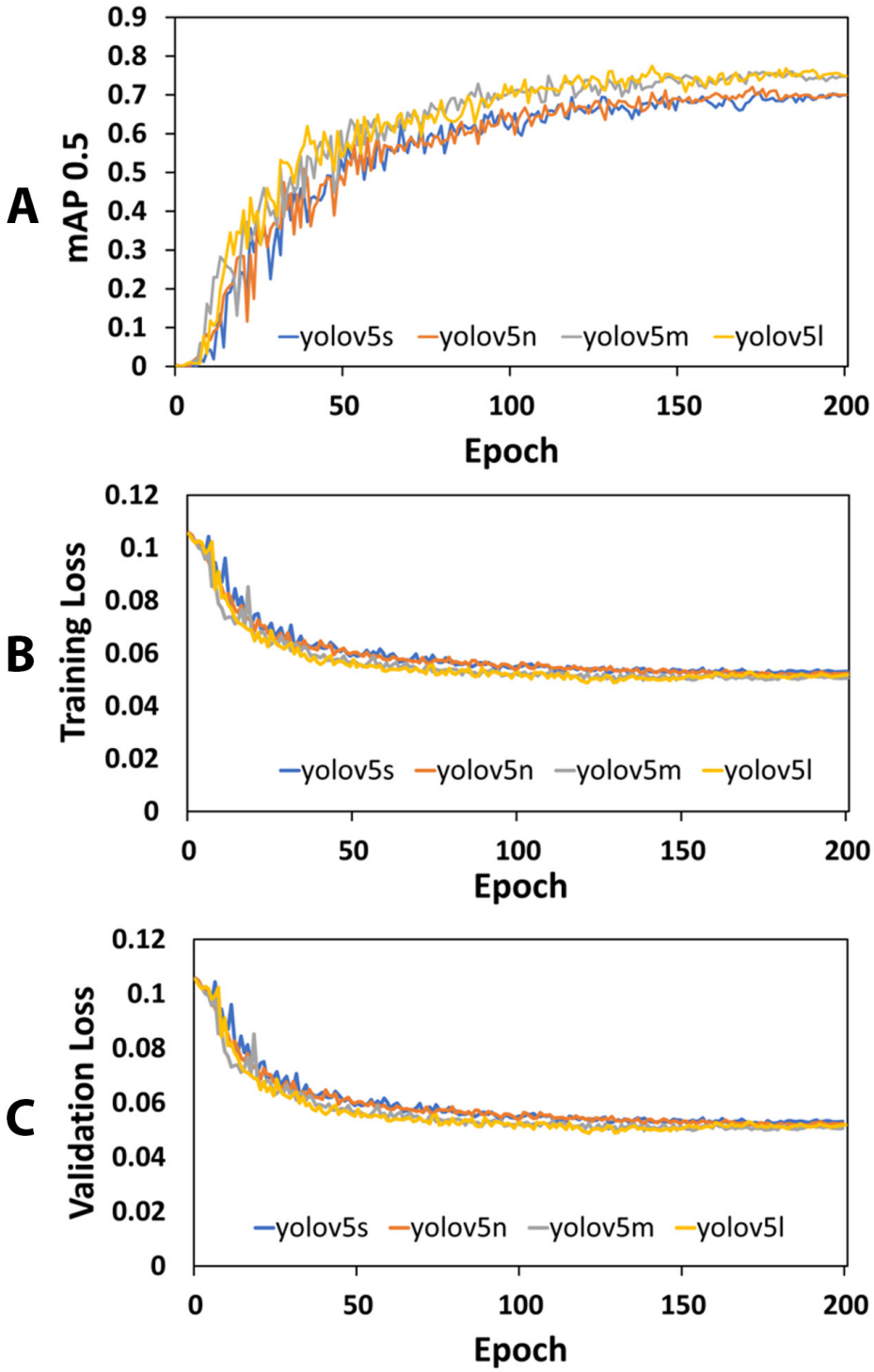

Figure 7: Mean average precision at the intersection over union threshold 0.5 throughout the 200 epochs each model was trained on (A). Training loss of each model throughout 200 epochs (B), and the validation loss of each model throughout 200 epochs (C). As the model trains for more epochs, it slowly improves by increasing the mAP and decreasing the loss.

3.3.2 Trash Detection Model Deployment

Because the AUV was tested using HIL, it produced no real footage to run through the trash detection model. To evaluate the abilities of the model, open-source footage was collected from the Japan Agency of Marine-Earth Science and Technology (JAMSTEC) HYPER-DOLPHIN submersible (HYPER-DOLPHIN n.d.). The model detected a total of 174,734 litter objects at depths of 500–800 m below the surface. Referring to Figure 8, the validation process produced a confidence-precision curve, which indicated that a confidence threshold of 0.4 could be established to attain a precision level of 80%.

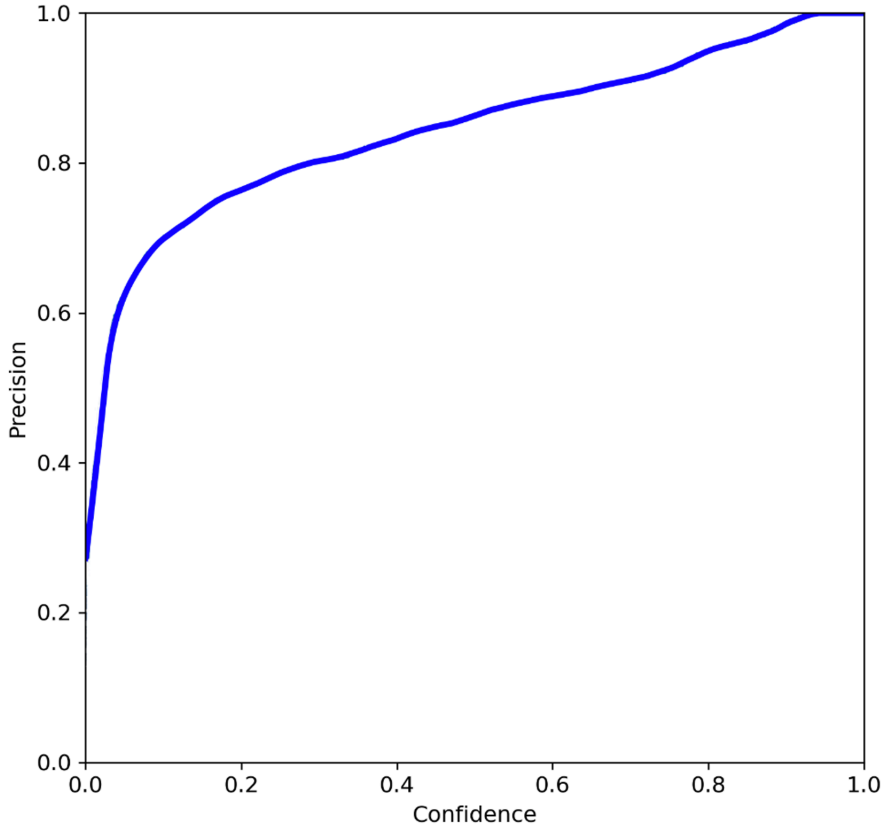

Figure 8: Confidence vs. precision of the YOLOv5l model. A confidence level of 0.4 was chosen to achieve a model precision of 80%.

Figure 9 shows the model inferencing a frame from the submersible and the detected objects from the model deployment.

4 CONCLUSION AND FUTURE WORK

This study shows an engineered AUV along with the training and deployment of a trash detection model. As shown by the HIL tests, the AUV can accurately read sensor data and process footage while navigating underwater, and the high precision of the computer vision model can seamlessly detect and analyze litter within underwater footage. The test on the prototype AUV and the trash detection computer model indicate that this system would be a viable method to quantify and map litter concentrations across our world's seas.

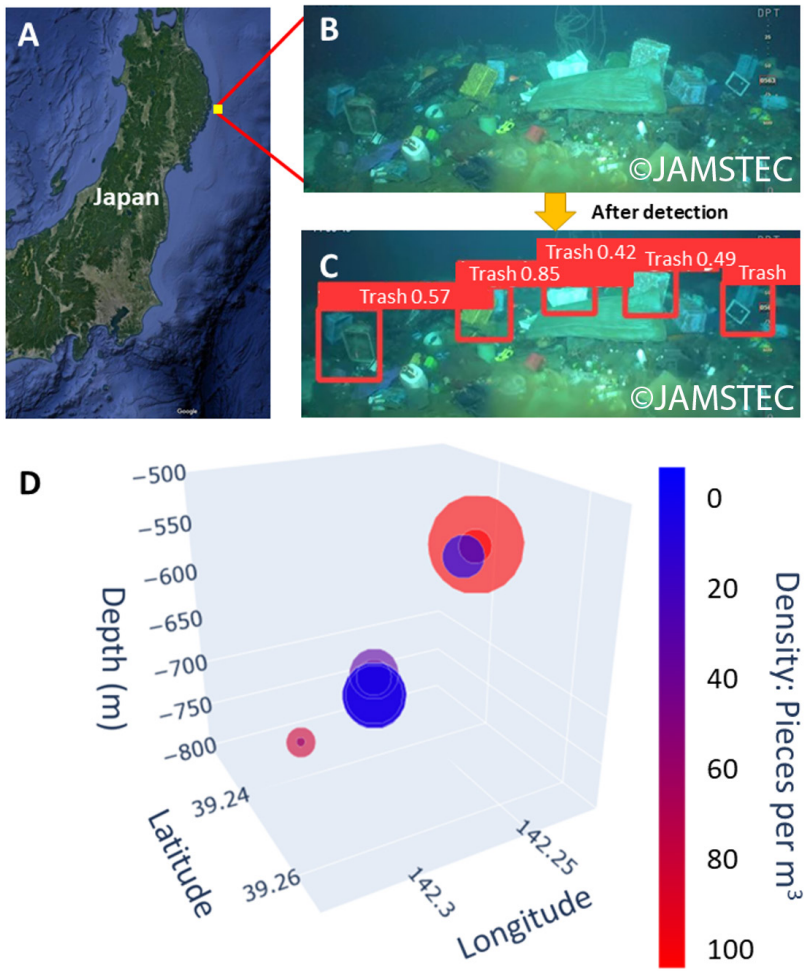

Figure 9: (A) Location of the footage collected from the submersible off the coast of Kamaishi. Map data © 2023 Google. (B) Raw footage from the submersible. Reproduced with permission from JAMSTEC. Copyright 2014 JAMSTEC. (C) Inferenced image after being processed by the YOLOv5l trash detection model. Reproduced with permission from JAMSTEC. Copyright 2014 JAMSTEC. (D) Areas of debris detected by the model and the relative density of litter in each area represented by color.

With HIL simulation, the AUV demonstrated the ability to collect sensor data and operate in underwater conditions. At the same time, the trash detection model found 174,000 debris objects underwater at depths of 500–800 m below the surface, a significant improvement to the 4000 litter items discovered at depths of 300–600 meters by oceanic cruises in the Messina Strait (Pierdomenico et al., 2019). Through the field test, the prototype AUV's operational and data collection capabilities were assessed, showing that the AUV was able to perform basic movement functions while collecting data at a high sample rate of 5400 Hz.

An exploration into replacements for the external parts of the AUV (the outer shell of the vehicle in contact with the environment) could yield better materials to handle salty ocean conditions and the use of more durable plastics for 3D-printed parts could give the vehicle a more robust design. However, the biggest improvement is for more testing and evaluation to be done on the vehicle. Further tests in local bodies of water or even in the ocean could yield important flaws within the vehicle design. Furthermore, the accelerometer onboard the AUV could be used to measure the forces of ocean currents to track the movement of debris, rather than just the position.

Currently, the trash detection model has only one classification level and can only evaluate whether trash is in the image or not. By using a more comprehensive dataset during training, the model would be able to classify different types of debris (e.g., plastic, metal, glass). Furthermore, by tuning hyperparameters within the existing model (number of epochs, learning rate, and model architecture), the mAP and loss of the model can be improved.

AUTHOR INFORMATION

***Corresponding Author**

Daniel Kim
Los Alamos High School
1300 Diamond Drive
Los Alamos, New Mexico 87547
Email: daniel360kim@gmail.com

ACKNOWLEDGMENT

I would like to give thanks to Dr. Robert Hermes, a retiree from the Los Alamos National Laboratory, for his help in acquiring lead weights used in this study. Thank you to my parents for overseeing the many tests and evaluations required in this study.

REFERENCES

Andrady, A. L. Microplastics in the Marine Environment. *Marine Pollution Bulletin* **2011**, *62* (8), 1596–1605. DOI:10.1016/j.marpolbul.2011.05.030.

Backhurst, M. K.; Cole, R. G. Subtidal Benthic Marine Litter at Kawau Island, North-Eastern New Zealand. *Journal of Environmental Management* **2000**, *60* (3), 227–237. DOI:10.1006/jema.2000.0381.

Barshan, B.; Durrant-Whyte, H. F. Inertial Navigation Systems for Mobile Robots. *IEEE Transactions on Robotics and Automation* **1995**, *11* (3), 328–342. DOI:10.1109/70.388775.

Beaumont, N. J.; Aanesen, M.; Austen, M. C.; Börger, T.; Clark, J. R.; Cole, M.; Hooper, T.; Lindeque, P. K.; Pascoe, C.; Wyles, K. J. Global Ecological, Social and Economic Impacts of Marine Plastic. *Marine Pollution Bulletin* **2019**, *142*, 189–195. DOI:10.1016/j.marpolbul.2019.03.022.

Beitzel, S. M.; Jensen, E. C.; Frieder, O. MAP. *Encyclopedia of Database Systems* **2009**, 1691–1692. DOI:10.1007/978-0-387-39940-9_492.

Cortex-M7. developer.arm.com. https://developer.arm.com/Processors/Cortex-M7 (accessed 2022-12-18).

Eiler, J. H.; Grothues, T. M.; Dobarro, J. A.; Masuda, M. M. Comparing Autonomous Underwater Vehicle (AUV) and Vessel-Based Tracking Performance for Locating Acoustically Tagged Fish. *Marine Fisheries Review* **2013**, *75* (4), 27–42. DOI:10.7755/mfr.75.4.2.

Eriksen, M.; Lebreton, L. C.; Carson, H. S.; Thiel, M.; Moore, C. J.; Borerro, J. C.; Galgani, F.; Ryan, P. G.; Reisser, J. Plastic Pollution in the World's Oceans: More than 5 Trillion Plastic Pieces Weighing over 250,000 Tons Afloat at Sea. *PLoS ONE* **2014**, *9* (12). DOI:10.1371/journal.pone.0111913.

Foxlin, E. Inertial head-tracker sensor fusion by a complementary separate-bias Kalman filter. In **Proceedings of the IEEE 1996 Virtual Reality Annual International Symposium**, Santa Clara, CA, United States, 1996; pp 185–194. DOI:10.1109/VRAIS.1996.490527.

Fulton, M.; Hong, J.; Islam, M.J.; Satta, J. Robotic Detection of Marine Litter Using Deep Visual Detection Models. In **2019 International Conference on Robotics and Automation (ICRA)**, Monetreal, QC, Canada, 2019; pp 5752–5758. DOI: 10.1109/ICRA.2019.8793975.

Galgani, F. Marine Litter, Future Prospects for Research. *Frontiers in Marine Science* **2015**, *2*. DOI:10.3389/fmars.2015.00087.

Galloway, T. S.; Cole, M.; Lewis, C. Interactions of Microplastic Debris throughout the Marine Ecosystem. *Nature Ecology & Evolution* **2017**. DOI:10.1038/s41559-017-0116.

Geyer, R.; Jambeck, J. R.; Law, K. L. Production, Use, and Fate of All Plastics Ever Made. *Science Advances* **2017**, *3* (7). DOI:10.1126/sciadv.1700782.

HYPER-DOLPHIN. www.jamstec.go.jp. https://www.jamstec.go.jp/e/about/equipment/ships/hyperdolphin.html (accessed 2024-01-12).

JAMSTEC - JAPAN AGENCY FOR MARINE-EARTH SCIENCE AND TECHNOLOGY. www.jamstec.go.jp. https://www.jamstec.go.jp/e/ (accessed 2023-12-27).

Jocher, G. YOLOv5. GitHub. https://github.com/ultralytics/yolov5 (accessed 2022-12-18).

Kalman, R. E. A New Approach to Linear Filtering and Prediction Problems. *Journal of Basic Engineering* **1960**, *82* (1), 35–45. DOI:10.1115/1.3662552.

Katsanevakis, S.; Verriopoulos, G.; Nicolaidou, A.; Thessalou-Legaki, M. Effect of Marine Litter on the Benthic Megafauna of Coastal Soft Bottoms: A Manipulative Field Experiment. *Marine Pollution Bulletin* **2007**, *54* (6), 771–778. DOI:10.1016/j.marpolbul.2006.12.016.

Lebreton, L.; Slat, B.; Ferrari, F.; Sainte-Rose, B.; Aitken, J.; Marthouse, R.; Hajbane, S.; Cunsolo, S.; Schwarz, A.; Levivier, A.; Noble, K.; Debeljak, P.; Maral, H.; Schoeneich-Argent, R.; Brambini, R.; Reisser, J. Evidence That the Great Pacific Garbage Patch Is Rapidly Accumulating Plastic. *Scientific Reports* **2018**, *8* (1). DOI:10.1038/s41598-018-22939-w.

Long Range AUV (LRAUV). MBARI. https://www.mbari.org/technology/long-range-auv-lrauv (accessed 2023-11-07).

Luinge, H. J.; Veltink, P. H.; Baten, C. T. M. Estimation of orientation with gyroscopes and accelerometers. In **Proceedings of the First Joint BMES/EMBS Conference. 1999 IEEE Engineering in Medicine and Biology 21st Annual Conference and the 1999 Annual Fall Meeting of the Biomedical Engineering Society**, Atlanta, CA, United States, 1999; Vol. 2, pp 844. DOI: 10.1109/IEMBS.1999.803999.

Madgwick, S. O. H.; Harrison, A. J. L.; Vaidyanathan, R. Estimation of IMU and MARG orientation using a gradient descent algorithm. In **2011 IEEE International Conference on Rehabilitation Robotics**, Zurich, Switzerland, 2011; pp 1–7. DOI:10.1109/ICORR.2011.5975346.

Marins, J. L.; Yun, X.; Bachmann, E. R.; McGhee, R. B.; Zyda, M. J. An extended Kalman filter for quaternion-based orientation estimation using MARG sensors. In **Proceedings 2001 IEEE/RSJ International Conference on Intelligent Robots and Systems. Expanding the Societal Role of Robotics in the the Next Millennium**, Maui, HI, United States, 2001; Vol. 4, pp 2003–2011. DOI: 10.1109/IROS.2001.976367.

Palaseanu-Lovejoy, M.; Alexandrov, O.; Danielson, J.; Storlazzi, C. Satsead: Satellite Triangulated Sea Depth Open-Source Bathymetry Module for NASA Ames Stereo Pipeline. *Remote Sensing* **2023**, *15* (16), 3950. DOI:10.3390/rs15163950.

Parker, L. Ocean Trash: 5.25 Trillion Pieces and Counting, but Big Questions Remain | National Geographic Society. education.nationalgeographic.org. https://education.nationalgeographic.org/resource/ocean-trash-525-trillion-pieces-and-counting-big-questions-remain (accessed 2022-12-18).

Pierdomenico, M.; Casalbore, D.; Chiocci, F. L. Massive Benthic Litter Funnelled to Deep Sea by Flash-Flood Generated Hyperpycnal Flows. *Scientific Reports* **2019**, *9*. DOI:10.1038/s41598-019-41816-8.

Powell, A.; Clarke, M. E.; Haltuch, M. A.; Fruh, E.; Anderson, J.; Whitmire, C. E.; Johnson, M. M. First Autonomous Underwater Vehicle Observations of a Potential Petrale Sole (Eopsetta Jordani) Spawning Aggregation off the US West Coast. *Frontiers in Marine Science* **2022**, *9*. DOI:10.3389/fmars.2022.834839.

Qureshi, U.; Shaikh, F.; Aziz, Z.; Shah, S.; Sheikh, A.; Felemban, E.; Qaisar, S. RF Path and Absorption Loss Estimation for Underwater Wireless Sensor Networks in Different Water Environments. *Sensors* **2016**, *16* (6), 890. DOI:10.3390/s16060890.

Schofield, O.; Kohut, J.; Aragon, D.; Creed, L.; Graver, J.; Haldeman, C.; Kerfoot, J.; Roarty, H.; Jones, C.; Webb, D.; Glenn, S. Slocum Gliders: Robust and Ready. *Journal of Field Robotics* **2007**, *24* (6), 473–485. DOI:10.1002/rob.20200.

Seafloor Mapping AUV. MBARI. https://www.mbari.org/technology/seafloor-mapping-auv (accessed 2023-11-07).

Stefatos, A.; Charalampakis, M.; Papatheodorou, G.; Ferentinos, G. Marine Debris on the Seafloor of the Mediterranean Sea: Examples from Two Enclosed Gulfs in Western Greece. *Marine Pollution Bulletin* **1999**, *38* (5), 389–393. DOI:10.1016/s0025-326x(98)00141-6.

Teensy® 4.1. www.pjrc.com. https://www.pjrc.com/store/teensy41.html (accessed 2022-12-18).

What Is Hardware-in-the-Loop? www.ni.com. https://www.ni.com/en/solutions/transportation/hardware-in-the-loop/what-is-hardware-in-the-loop-.html (accessed 2022-12-18).